Tanzania Journal of Science 50(2): 334-346, 2024
ISSN 0856-1761, e-ISSN 2507-7961

Assessment of Onshore Wind Farm Performance to Geometric Layout Choices by Utilizing Mesoscale Modelling Techniques

Rajabu Juma Mangara[1, 2*] and Laban Lameck Kebacho[1, 2]

[1]*Physics Department, College of Natural and Applied Sciences, University of Dar es Salaam, P.O. Box 35063, Dar es Salaam, Tanzania.*

[2]*Environmental and Atmospheric Sciences Group, Physics Department, University of Dar es Salaam, Tanzania.*

*E-mails: rajyjuma@yahoo.com, *mangara.rajabu@udsm.ac.tz, kebacho.laban@gmail.com*

Received 16 Jan 2024, Revised 29 March 2024, Accepted, Published June 2024

*****Corresponding author

https://dx.doi.org/10.4314/tjs.v50i2.13

Abstract

Previous studies have shown that the average losses of wind power production due to the wind turbine wake effect within operating wind farms is between 10% to 20% of the overall power output. Among other factors, it is reviled that, the wind farm array layout can contribute significantly to both wake effect and power loss at the wind farm site. This study employs mesoscale modelling techniques to assess the effect of geometric layout on the onshore wind farms performance. Geometric layout can be defined by the spacing and alignment (e.g. staggered or aligned) of the wind turbines with respect to the prevailing wind direction. The Weather Research and Forecasting (WRF) model in this study utilised Fitch's wind farm parameterization to simulate the interaction between wind turbine blades rotation and the atmosphere. To examine a wide range of operating conditions observed within the real-world operating wind farms, two idealised numerical simulations are carried out for each designed wind farm geometric layout, one with the convective condition and another with stable condition. Among the four different designed wind farm geometric layouts, the triangular wind farm layout which offered staggering after every next row was noted to be the easiest method for improving the wind farm performance by increasing the capacity factor from 0.55 to 0.71 and decreasing array losses from 9.15 % to 4.63 %. Comparison between stable and convective regime indicates that the highest capacity factor was obtained during the stable case with the highest power loss owing to increased wake impacts downstream. The lowest value of the capacity factor was obtained during the convective case with the lowest power loss for both four designed wind farms.

Keywords: Wake effect; Wind farm parameterization; Modelling; Capacity factor; Turbulent kinetic energy.

Introduction

To offset the recent observed anthropogenic climate change, the global dependence on fossil fuels is dropping amid renewable energy sources. As the fast-growing renewable energy source, wind energy cumulative installed capacity rose from 23.9 GW in 2001 to 906 GW in 2022 and forecasted that 1221 GW of new capacity will be added between 2023 and 2030 (GWEC 2023). Because of the large development experienced within wind energy industry, considerable efforts have been directed on the improvement of the performance of wind farms (Fitch et al. 2012). The geometric of the wind turbines layout within the wind farm reported to affect its performance. Poor design of the layout can lead to wind farm power

deficits and increase operation and maintenance costs of the wind farm (Kusiak and Song, 2010). This may hinder the development of the renewable energy sector.

The wind turbines withdraw momentum from the atmospheric flow; thus, the downstream wind turbines suffer wind speed deficit relative to the upstream and elevate turbulence intensity (Barthelmie et. al. 2013). This phenomenon is well known as wake effect. The recovery of the wake effect occurs when air is drawn in from the surrounding flow. In the wind farm (large arrays), downstream wind turbines experience the wake effect due to upstream wind turbines as a results of output power deficits and dynamic loading due to the increased turbulence intensity. Thus, as the wind farms become large in size and increase in numbers, accurately quantifying of the interactions between wind turbines and the atmosphere become among the recent research challenges.

The wake effect from upstream wind turbines causes wind speed deficit for downstream wind turbines. Consequently, the power output of the downstream wind turbines become lower than the upstream wind turbines of the same kind. Because conventional wind turbines' geometric layout significantly increases the wake effect, geometric layout optimization during wind project designing stage can be a rational strategy to improve the wind farm performance. For these purposes, different modelling approaches have been proposed (Barthelmie et al. 2010, Larsen et al. 2008, and Pedro et al. 2015). All these studies have quantified the wind farm power production and its associated wake effect. These studies quantified the average power deficit due to the wake effect of the order of 10% and 20% of total wind farm power output. Among other factors, the wind farm geometric layout can contribute significantly to the wake effect and power loss within the wind farm Pedro et al. (2015), and therefore it is important to consider it during the wind farm design stage. Wind farm variables considered during design stage includes: number of wind turbines; the wind farm size and geometric shape; the wind turbine model and diameter; spacing between wind turbines; alignment of the wind turbines; and orientation of the rows for the predominant wind direction (Archer et al. 2014).

In recent years, two parameterizations of wind farm for mesoscale numerical models were introduced by Fitch et al. (2012) and Volker et al. (2015). Both of them represent the wind turbine rotor as a raised momentum deficit, but the turbulent kinetic energy (TKE) effect of the wind turbines is captured differently. While Fitch et al. (2012) added TKE direct at the rotor height by considering power coefficient and thrust, Volker et al. (2015) allows TKE to evolve from the momentum field. Fitch's wind farm parameterization now is commonly available with the Weather Research and Forecasting (WRF) model which is popular to the scientific community. One of the advantages of the WRF mesoscale model is that it is capable of running in both idealised and real-world configurations. In the idealised configuration, user can customize all forcing conditions while in real-world configuration, the reanalysis data from large models and observations data are used to force the WRF model run (Skamarock et al. 2021). The WRF equipped with wind farm parameterizations (WFPs) can represent the complexity interaction between wind turbines and atmospheric processes. The benefits of using the WRF model on a mesoscale wind energy study have been discussed by Fitch et al. (2012) and Mangara et al. (2019). Primarily, the WFPs in WRF model is introduced to study the wind farms impact on regional and global scales. However, now days it also used to optimize the wind farm power output (e.g., Jimenez et al. 2015, Vanderwende et al. 2016) particularly for large-scale wind energy uncertainties such as grid balancing (Archer and Jacobson 2007, St. Martin et al. 2015) and interactions among wind farms (Kaffine and Worley 2010, Nygaard 2014).

In this study, the assessment of wind farm performance sensitivity to geometric layout options is examined by different parameters. Therefore, this study quantifies the advantages and disadvantages of selected geometric layout options. The results will be important to the wind energy sector by optimising wind

power output. The performance of the alternative wind farm layouts quantified via array performance with respect to number of wind turbines, capacity factor, and total power array losses can eventually be transformed to actual costs or savings.

Material and Methods

Designed Wind Farm Geometric Shapes

To evaluates the wind farm geometric layouts performance, four different wind farm geometric shapes are designed as represented in Figure 1. Each wind farm has 36 wind turbines and 54 MW theoretical wind power capacity. The configurations of the 1.5-MW SINOVEL SL1500/89 wind turbines in a similar way as in Mangara et al. 2019 were used. The first layout is a square wind farm (SQF) with 6 by 6 wind turbines and the second one is an equilateral triangular wind farm (TRF) layout with 8 wind turbines on each side and the base facing the prevailing wind direction. The subsequent rows in TRF are staggered in such a way that each succeeding row has wind turbines placed within gaps of the previous row. The third is vertical rectangular layout (VTF) with 4 by 9 wind turbines and the widest side facing the prevailing wind direction. The last one is the horizontal rectangular layout (HRF), with the narrow side facing the prevailing wind direction.

With the wind farm layouts characteristics defined, it is essential to establish model domain for the idealised simulations. A 42 by 42 model grids, with 500 m spacing (horizontal resolution) is used, which makes the total domain 21 by 21 km. The idealised model runs are integrated with 5 s time steps. The wind farms are placed at the centre of the model domain such that the wind turbine rows and columns are spaced about 500 m apart (equivalent to 6 rotor diameter), therefore the wind turbines spacing in both the zonal and meridional directions are equivalent to grid spacing.

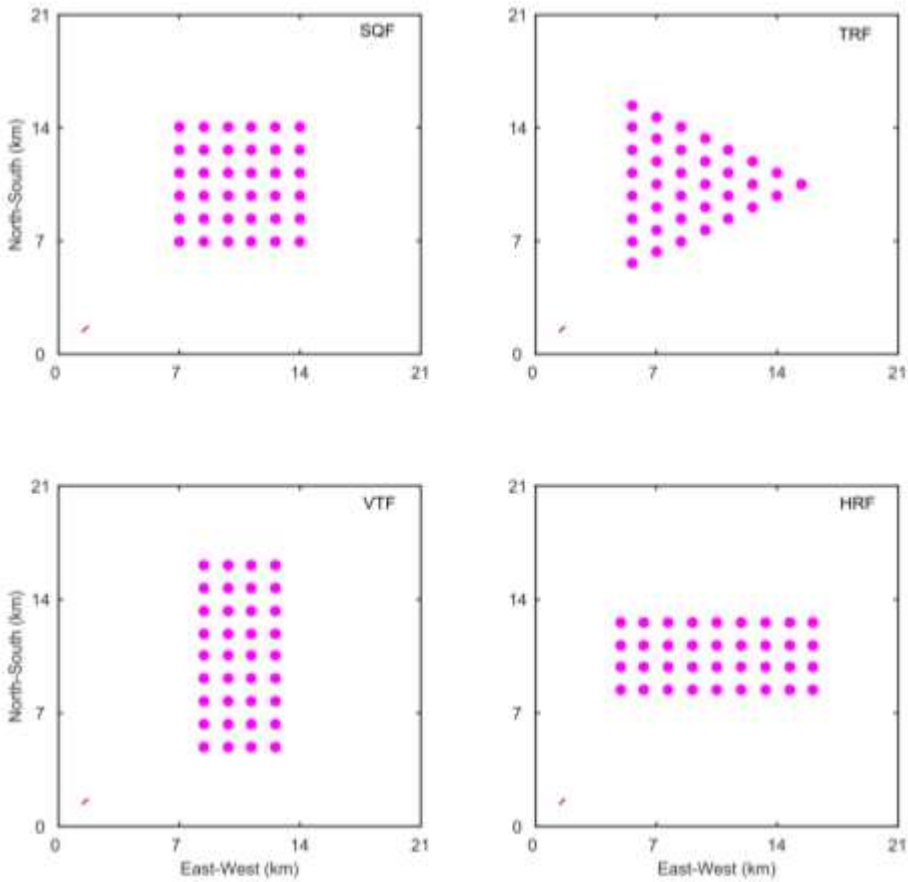

Figure 1: The four schematic geometric wind farm arrays used in the idealised WRF numerical simulations, with coloured filled circles representing wind turbines.

Model Configurations

The model was configured to have 51 vertical levels which extends up to 12 km. The lowermost layer at the beginning of the model simulations occurs at about 19 m above the surface. About 27 vertical levels are spaced under 300 m (approximately 11 m vertical grid spacing), with the levels getting thicker into the higher atmosphere. The real position of each vertical level varies with time as it can be calculated from the geopotential height. The model surface is characterised as flat terrain with a surface albedo of 0.16 and aerodynamic roughness length of 0.008 m (Skamarock et al. 2021). The idealised WRF model runs for 2 hours, with a uniform zonal wind speed, u = 12 m/s and meridional wind speed, v = 0 m/s at all vertical levels throughout the domain. The 2 hours was chosen as an illustrative time for the model performance. The wind speeds at the wind farm site were chosen to be high enough for the rated performance of the wind turbines, but cannot ignore the wake effects on wind power generation of the downstream wind turbines. Within the first 15 minutes of the model run, the model began to show a wake pattern from the wind farms and continued throughout the model simulation time.

To achieve the objective of this study, the em_seabreeze2d_x idealised case was used to perform all the experiments. This mesoscale WRF idealised case, allows to perform a simple sea or land breeze simulation in 2D (x and z directions). The sea component from the parameterization scheme is removed and the

domain extended into 3D (x, y, and z) to create an idealised onshore flat terrain environment within which the wind farm can be modelled. The model was configured with physical schemes appropriate for the study of wind farm dynamics. The Mellor-Yamada-Nakanishi-Niino (MYNN) Level 2.5 planetary boundary layer scheme was chosen to handle the boundary layer physics (Nakanishi and Niino 2006). This scheme contains pressure covariance and buoyancy for parameterizing mixing length scale which is important for the wind farm parameterization. Thus, when combined with the 1.5 TKE closure scheme, it allows an enhancement of the wind farm parameterization as described by Fitch et al. 2012. The mesoscale idealised WRF model was performed without moisture, cumulus, microphysics, radiation, and land-surface schemes (Mirocha et al. 2014, Aitken et al. 2014, Vanderwende et al. 2016).

To examine a wide range of operating conditions observed within the real-world operating wind farms (e.g., Rejewski et al. 2013, Vanderwende and Lundquist 2012), two idealised numerical simulations were carried out for each designed wind farm geometric layout, one with the convective (unstable) condition and another with stable condition. These idealised model simulations are configured in a similar way with Mirocha et al. (2014) and Aitken et al. (2014) for the stable and unstable (convective) case, respectively. The unstable (convective) condition is defined as in Vanderwende et al. (2016) with surface heat flux of 100 W m^{-1}. The stable condition was obtained following Aitken et al. (2014) and Vanderwende et al. (2016) by maintaining a surface cooling rate of 0.2 K h^{-1}. In both cases of the idealised model simulations, the temperature inversion was set to be 10 K km^{-1} and a Rayleigh damping layer was used to prevent the turbulence from reaching the highest vertical level model domain.

Analysis of the Model Output

There are various approaches used to assess the performance of the simulated wind farm, each provides different information. The first method is the direct comparison of the total wind power output computed from the model output (Fitch et al. 2012, 2013a, Lee and Lundquist 2017). The second method is by considering the wind farm capacity factor (*CF*) as well as power loss (*PL*) within the wind farm operation site (Barthelmie and Jensen 2010, Barthelmie et al. 2010, Archer et al. 2013, Peña et al. 2018). The *CF* is defined as the total power output from all the wind turbines per maximum rated power of the wind farm and is given by equation 1.

$$CF = \frac{\sum_i P_i}{n_t P_R} \qquad 1$$

where P_i is the simulated power output of each wind turbine in the wind farm, P_R is the rated power of each wind turbine, and n_t is the number of wind turbines at the wind farm site. Normally, the capacity factor ranges from 0 to 1, or is rarely expressed in terms of percentage. Due to the wind speed deficit experienced within the wind farms, practically the capacity factor of a wind farm cannot reach the value 1, or 100 %. The capacity factor is used to determine the productivity of the wind farm for any given time or interval. The corresponding *PL* in equation 2 is defined by Peña et al. (2018):

$$PL = \left(1 - \frac{\left\langle \sum_i P_i \right\rangle}{n_t P_F}\right) \times 100\% \qquad 2$$

where P_F is defined as the power output from the wind farm assuming all turbines work at its rated capacity without the wake effect, and angle brackets represent the ensemble average of the simulated power output. In this subsection, both three mentioned methods (direct power production, capacity factor and power loss) were used to assess the performance of the four designed wind farm geometric layouts.

Results and Discussions

The wind speed at hub height (70 m above the ground) is extracted from the model simulation outputs to examine the performance of the designed wind farms. Significant difference observed in wake structure between the designed wind farm geometric layouts. The contours of average hub height wind speeds within the simulation domain observed after 2 hours of model simulation for stable and unstable regimes are shown in Figure 2 and 3, respectively. These contours cover an area encompassed by the inflow wind regime, wind turbines layout, and outflow wind regime. The right and left sides of the plots correspond to the upstream and downstream edges of the model simulation domain, respectively. Wind speed deficit due to the wake effect from the upstream wind turbines influences the inflow of downstream wind turbines in both stable and unstable regimes. Significant wake effect extends further downstream in the stable case (Figure 2) compared with the unstable regime (Figure 3). This is expected as the turbulent mixing is strongest in the convective (unstable) case which erodes wakes, consequently, reducing the downstream propagation distance of the noticeable wake effects. Also, the turbulent mixing influences downstream lateral interaction of the wakes for convective model simulation. On both two stability regimes, it can be noted that the HRF experiences significant wake effects with the maximum wind speed deficit inside the wind farm, and the TRF suffer the least wake effects with the minimum wind speed deficit within the wind farm.

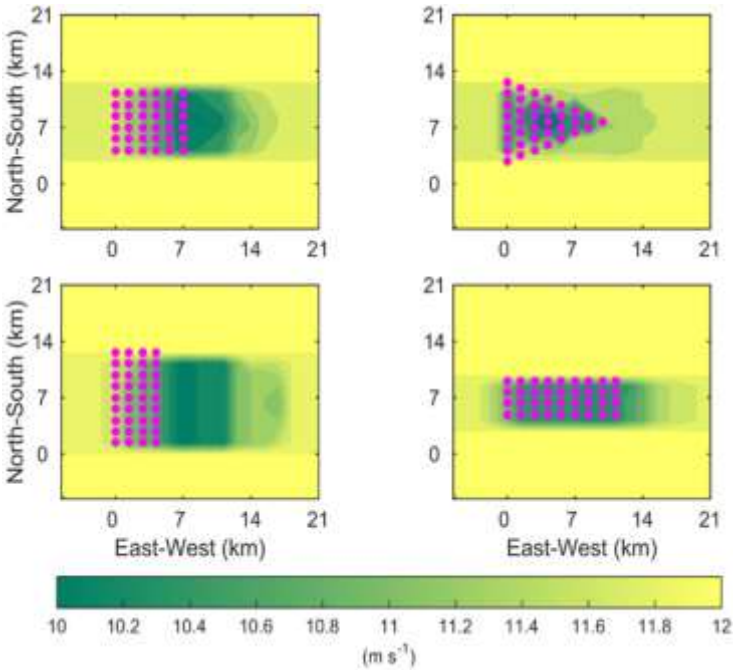

Figure 2: The idealised WRF model output for the four designed wind farms for stable boundary layer condition.

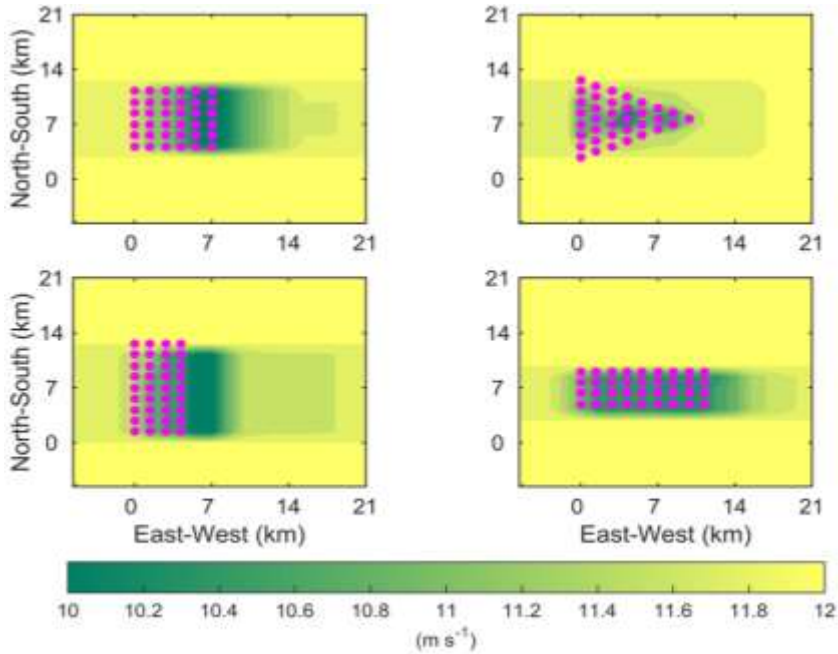

Figure 3: The idealised WRF model output for the four designed wind farms for convective boundary layer condition.

Figure 4 shows wind speed deficit (ΔWS) and excess turbulent kinetic energy (ΔTKE) vertical profiles between the upstream and the wind farm averaged area for convective and stable regimes. The model simulations in both two regimes produced wind speed profiles which agree with the atmospheric boundary layer theory established by Stull. (1988). As predicted, maximum wind speed deficit was noted during stable condition (Figure 4a), as turbulent mixing during convective regime erodes wakes more rapidly. Maximum wake effects occurred around the hub height during the stable atmospheric condition, and at upper half of the rotor layer around 100 m above the ground level during the convective case. The enhanced turbulent mixing of high momentum air downward, and pressure perturbations which channel the winds below the turbines rotor disc results in flow acceleration under the rotor during stable model simulation. This phenomenon also noted in operating wind farm observations by Rejewski et al. (2014), and Vanderwende et al. (2016) have reported a similar trend. At hub height in both two stability regimes, HRF produced large wind speed deficits compared with the rest of wind farm designs. Contrary, the TRF layout produces the least wind speed deficits.

The difference on the wind farm TKE production increased between the designed wind farm geometric layouts, as presented in Figure 4(b) and 4(d). The increase in TKE production occurred more rapidly in the stable atmospheric condition (Figure 4(d)) relative to the convective condition. Consistency with wind speed, the TKE production is lowest in TRF wind farm geometric design compared to the rest in both two model simulation stability regimes. Specifically, the staggering of the wind turbines within the wind farm optimizes the extraction of kinetic energy from the atmospheric flow compared with the aligned layout. However, the TKE production within the boundary layer is larger in the aligned layout compared with the staggered layout configuration. This is because in the aligned configurations the atmospheric flow is more heterogeneous compared with the staggered counterparts, which facilitate the mechanical boundary layer (shear) production of TKE. Note that data are presented as a difference between upstream and the wind farm average area for the 4 designed wind farm geometric

layout. Also, the horizontal blue line in Figure 4(a, b, c and d) denotes the wind turbines hub height; while the lower and upper horizontal dashed blue lines denote the lower and upper borders of the rotor disc, respectively.

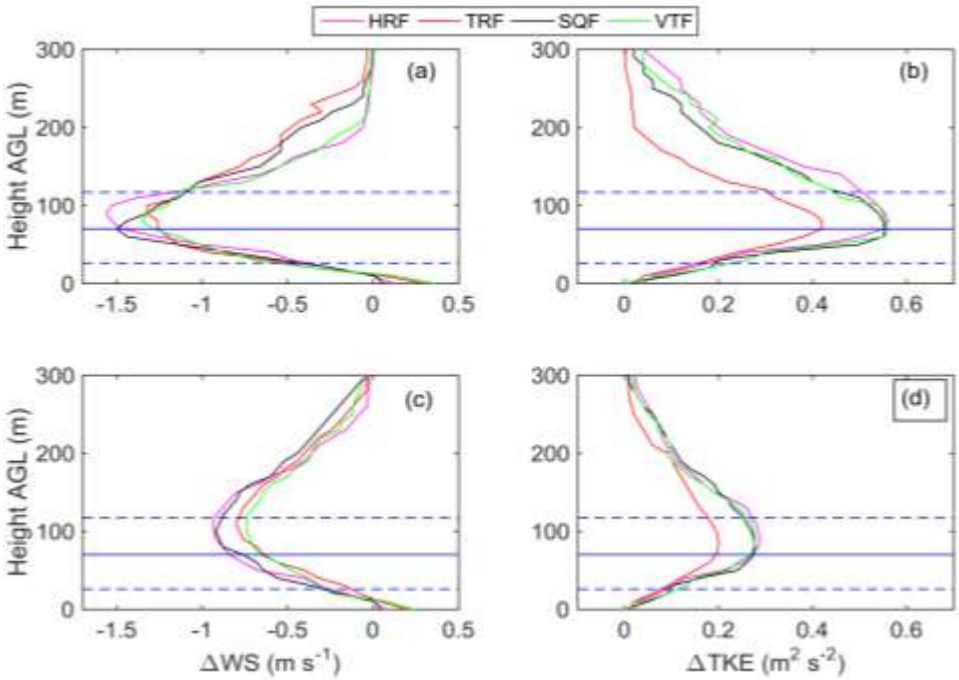

Figure 4: Low-level profiles for (a) wind speed deficits for the stable regime, (b) turbulent kinetic energy enhancement for stable regime, (c) wind speed deficits for the convective regime, and (d) turbulent kinetic energy enhancement for the convective regime.

The disagreement occurred between convective and stable regimes for the SQF and the VTF designed wind farm geometric arrays. In the stable conditions, the TKE production is higher in the VTF than in the SQF (Figure 4(b)), while in convective model simulations, the TKE production is higher in the SQF than in the VTF wind farm geometric array (Figure 4(d)). The results show that the estimated vertical mixing by the parameterized TKE in the SQF during the model simulations does not properly represent the equivalent mixing caused by simulated TKE in the VTF model simulations. Similar to the wind speed deficits, the maximum TKE productions occurred around the hub height during the stable conditions and at the upper half of the rotor layer around 100 m above the ground level in convective atmospheric conditions.

The instantaneous power output of each wind turbine inside the wind farm is extracted, and by summing them, the total power production of each geometric layout configuration is obtained for the two cases (convective and stable cases). The power output values were calculated for both two cases by comparing grid-cell wind speeds with the SL1500/89 power curve to interpret wind speeds to its corresponding power output. The results are summarised in Tables 1 and2, respectively. As simulated from the wake effect patterns (Figure 2 and 3), the HRF experiences the most dramatic loss of power between the best and the worst-producing wind turbine, while the TRF suffers the least loss of power followed by the VTF. The TRF also produces the least power loss, with the VTF performing second best. This result is possibly directly connected to the staggering array of the TRF wind farm when compared to most of the other wind farm geometric layouts. This reduces the wind speed deficits due to the weak wake

effect on the succeeding columns of the wind turbines. This reason is contrary to the case of the HRF. A comparison between the SQF and VTF, shows that the VTF performs better than the SQF. This is because in the VTF only three columns suffer the wind speed deficits of the first column compared to five columns in the SQF.

Table 1: Power output from simulation results of the 4 designed geometric shapes of wind farms, using idealised WRF model for convective regime.

	SQF	TRF	VTF	HRF
Total Power Output (MW)	43.32	45.39	44.43	40.59
Best Turbine Power Output (MW)	1.37	1.37	1.37	1.37
Worst Turbine Power Output (MW)	1.04	1.17	1.06	0.93
% Loss from Best to Worst	24.09	14.60	22.63	32.12
% Loss compared with 54 MW	19.78	15.94	17.72	24.83

Table 2: Power output from simulation results of the 4 designed geometric shapes of wind farms, using idealised WRF model for a stable regime.

	SQF	TRF	VTF	HRF
Total Power Output (MW)	42.02	44.70	43.11	39.12
Best Turbine Power Output (MW)	1.31	1.32	1.31	1.31
Worst Turbine Power Output (MW)	0.98	1.11	1.01	0.90
% Loss from Best to Worst	25.19	15.91	22.90	31.30
% Loss compared with 54 MW	22.19	17.22	20.17	27.56

Figure 5 shows the relative power loss as the wakes propagate toward downstream the wind farms for the convective case (Figure 5(a)), and stable case (Figure 5(b)). All values show the percentage of wind power produced relative to the upstream wind turbine row. Similar to the results presented in Tables 1 and 2, Figure 5 shows that the power losses across the wind turbine arrays were small in the convective regime for all the wind farm geometric configurations in comparison with the stable regime. The total power loss in the convective regime did not exceed 23% by column 8 in any configuration of the convective regime. These results appear similar to previous observations in operating wind farms (Christiansen and Hasager 2005, Barthelmie et al. 2010) and modelling studies (Fitch et al. 2012, Vanderwende et al. 2016). However, herein the results indicate more linear decay compare with the ones reported by Barthelmie et al. (2010) and Vanderwende et al. (2016).

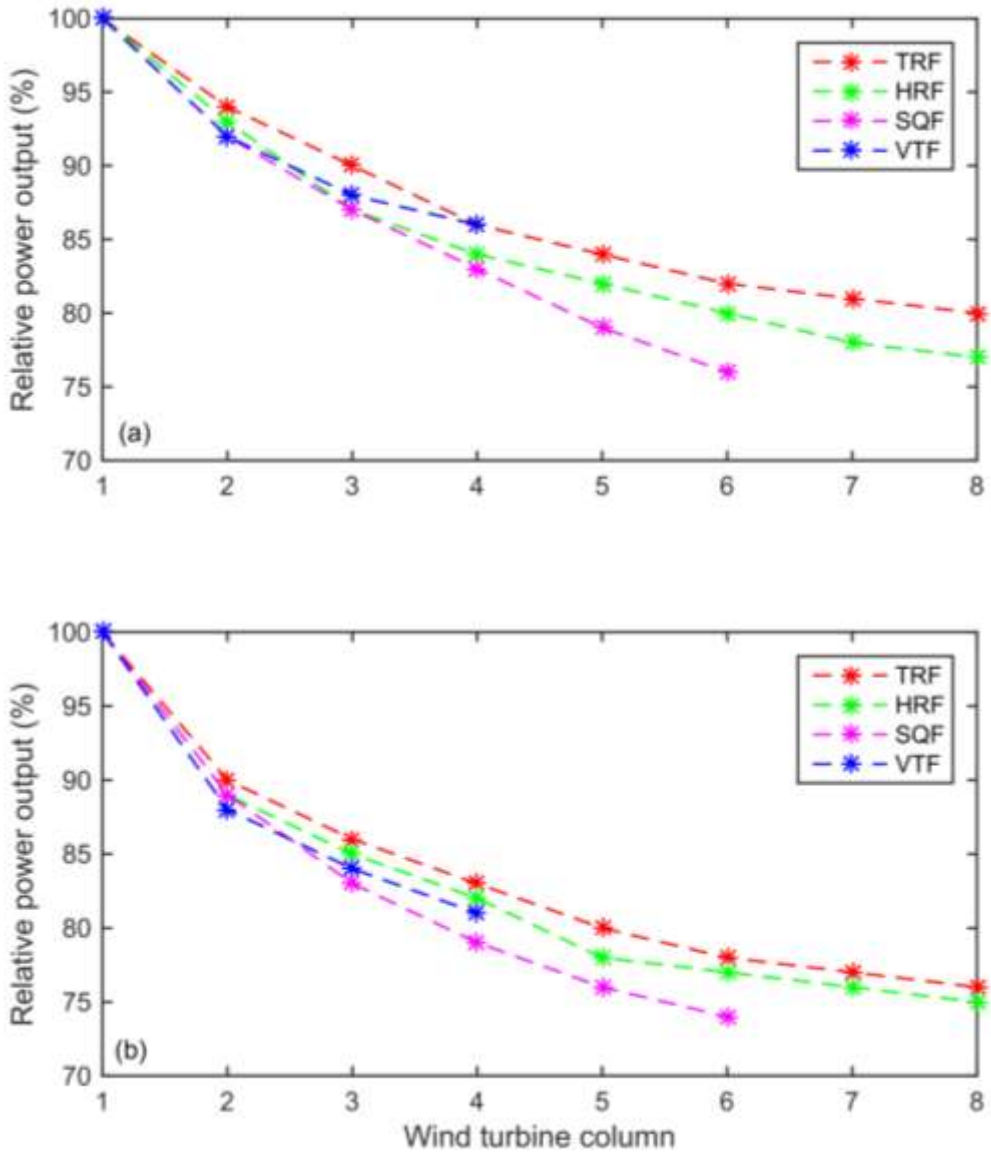

Figure 5: The power output along the centre row of each designed wind farm layout, relative to the power output of the initial upstream row (a) convective regime and (b) stable regime.

The capacity factors and power losses for the four designed wind farm geometric layouts are shown in Table 3. For both four designed wind farm layouts, the average capacity factor is greater than 0.5, and the corresponding average power loss is less than 10% for all four designed layouts. Similar to the total power output, the highest capacity factor is obtained during the stable case with the highest power loss owing to increased wake impacts downstream, and the lowest value of the capacity factor is obtained during the convective case with the lowest power loss for both four designed wind farms. This is due to the fact that, during the stable case, the highest wind speed is flowing within the rotor disc of the wind turbine with the highest value of the wind speed deficit, while the vice versa occurs

during the convective case.

Table 3: Estimated capacity factor and power loss of the four designed wind farm layouts for the simulation convective and stable cases.

	SQF		TRF		VTF		HRF	
	CF	*PL* (%)	*CF*	*PL* (%)	*CF*	*PL* (%)	*CF*	*PL* (%)
Stable case	0.64	8.28	0.77	6.01	0.70	7.99	0.61	11.10
Convective case	0.52	6.20	0.65	3.25	0.58	4.37	0.49	7.20
Average	0.58	7.24	0.71	4.63	0.64	6.18	0.55	9.15

The relationship between the two parameters namely capacity factor and power loss is shown in Figure 6. A comparison of the four designed wind farm layouts shows that the TRF gives the highest capacity factor and lowest power loss, and the HRF gives the lowest capacity factor and highest power loss. This result is similar to the total power production presented in this study.

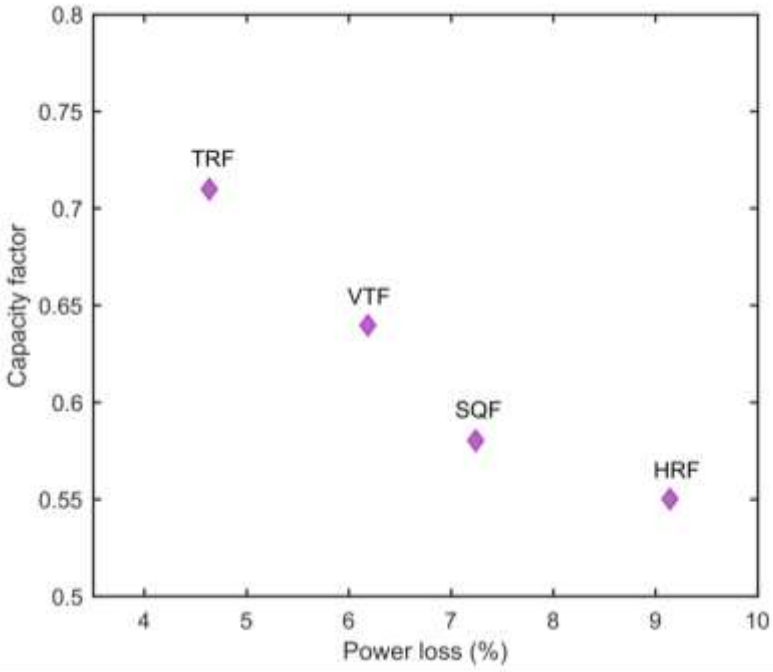

Figure 6: Relationship between the average capacity factor and power loss for the four designed wind farm geometric layouts (SQF, TRF, VTF, and HRF).

Conclusion

Studying the wake effects to make wind power more promising clean renewable energy is an indispensable topic all over the world in recent days. From the results presented herein, it can be noted that there is indeed a benefit in considering the geometric layout in designing the wind farm array layout to reduce the wake effects and improve performance of the wind farm. In this study, an idealised WRF model setup to assess the wake effects of 4 different wind farm

geometric layouts was described. The results indicated that both 4 designed wind farm layouts can influence wind power production. Furthermore, the results show that TRF suffered the least wake effects, with the highest capacity factor and wind power production compared to the others. This show that TRF wind farm geometric layout which establishes a staggering array outperformed the rest of the wind farms geometric layout designed in this study. Therefore, careful consideration of wind farm layout based on the local climatology can be useful to the overall wind power production. The described technique allows for assessing the possible wind power production of the suggested wind farm geometric layout under realistic meteorological conditions, by using a well-established and trusted numerical mesoscale model. Large-eddy simulations of these wind farms would provide more accurate wake effects and can resolve the wake effect of the individual wind turbines but at a high computational cost.

Acknowledgements

The authors acknowledge the support of the Department of Physics of the University of Dar es Salaam for the fund support given during the completion of this manuscript.

Conflict of Interest

The authors declare no conflict of interest in this research work.

References

Aitken ML, Kosovic B, Mirocha JD, and Lundquist JK 2014 Large eddy simulation of wind turbine wake dynamics in the stable boundary layer using the Weather Research and Forecasting Model. *J. Renew. Sustain. Energy.* 6(3):033137.

Archer CL, Colle BA, Delle Monache L, Dvorak MJ, Lundquist J, et al. 2014 Meteorology for Coastal/Offshore wind energy in the United States: Recommendations and research needs for the Next 10 Years. *Bul. Am. Meteo. Soc.*, 95(4):515-519.

Archer CL, Mirzaeisefat S, and Lee S 2013 Quantifying the sensitivity of wind farm performance to array layout options using large-eddy simulation. Geo. Res. Lett., 40(18):4963-4970.

Archer CL and Jacobson MZ 2007 Supplying baseload power and reducing transmission requirements by interconnecting wind farms. *J. Appl. Meteor. Clim.,* 46:1701-1717.

Barthelmie RJ, Hansen KS, and Pryor SC 2013 Meteorological controls on wind turbine wakes. *IEEE Proceed.* 101(4): 1010 – 1019.

Barthelmie RJ, Pryor SC, Frandsen ST, Schepers JG, Rados K, Schlez W, Neubert A, Jensen LE, and Neckelmann S 2010 Quantifying the impact of wind turbine wakes on power output at offshore wind farms. *J. Atmos. Ocea. Techn.*, 27(8):1302-1317.

Barthelmie RJ, and Jensen LE 2010 Evaluation of wind farm efficiency and wind turbine wakes at the Nysted offshore wind farm. *Wind Energy*, 13(6):573-586.

Christiansen MB, and Hasager CB 2005 Wake effects of large offshore wind farms identified from satellite SAR. *Rem. Sens. Env*., 98(3):251-268.

Fitch AC, Lundquist JK, and Olson JB 2013 Mesoscale influences of wind farms throughout a diurnal cycle. *Month Weather Rev.*, 141(7):2173-2198.

Fitch AC, Olson JB, Lundquist JK, Dudhia J, Gupta AK, Michalakes J, and Bastard I 2012 Local and mesoscale impacts of wind farms as parameterized in a mesoscale NWP model. *Mon. Weather Rev.* 140(4):3017-3038.

Global Wind Energy Council (GWEC) 2023 Global wind statistics 2022. *Global Wind Energy Council Rep*.

Jiménez PA, Navarro J, Palomares AM, and Dudhia J 2015 Mesoscale modeling of offshore wind turbine wakes at the wind farm resolving scale: a composite-based analysis with the Weather Research and Forecasting model over Horns Rev. *Wind Energy*, 18(3):559-566.

Kaffine DT, and Worley CM 2010 The windy commons? *Environ. Resour. Econ.* 47(2):151-172.

Kusiak A, and Song Z 2010 Design of wind farm layout for maximum wind energy capture. *Renew. Energy*, 35(3): 685-694.

Larsen GC, Madsen HA, Thomsen K, and Larsen TJ 2008 Wake meandering: a pragmatic approach. *Wind Energy* 11: 377–395.

Lee JC, and Lundquist JK 2017 Evaluation of the wind farm parameterization in the Weather Research and Forecasting model (version 3.8.1) with meteorological and turbine power data. *Geosc. Mod. Devel.* 10: 4229-4244.

Mangara RJ, Guo Z, and Li S 2019 Performance of the wind farm parameterization scheme coupled with the weather research and forecasting model under multiple resolution regimes for simulating an onshore wind farm. *Adv. Atmos. Sci.* 36(2):119-132.

Mirocha JD, Kosovic B, Aitken ML, and Lundquist JK 2014 Implementation of a generalized actuator disk wind turbine model into the weather research and forecasting model for large-eddy simulation applications. *J. Renew. Sustain. Energy.*, 6(1):013104.

Nakanishi M, and Niino H 2009 Development of an improved turbulence closure model for the atmospheric boundary layer. *J. Meteo. Soc. Jap.*, 87(5): 895-912.

Nygaard GN 2014 Wakes in very large wind farms and the effect of neighbouring wind farms. *J. Phys.: Conf. Ser.* 524:1-10.

Pedro AJ, Jorge N, Ana MP, and Dudhia J 2015 Mesoscale modeling of offshore wind turbine wakes at the wind farm resolving scale: a composite-based analysis with the weather research and forecasting model over Horns Rev. *Wind Energy* 18(3): 559-566.

Peña A, Hansen KS, Ott S, and van der Laan MP 2018 On wake modeling, wind-farm gradients, and AEP predictions at the Anholt wind farm. Wind Ener. Sci., 3:191–202.

Rajewski DA, Takle ES, Lundquist JK, Oncley S, Prueger JH, Horst TW, Rhodes ME, Pfeiffer R, Hatfield JL, Spoth KK and Doorenbos RK 2013 Crop Wind Energy Experiment (CWEX): Observations of Surface-Layer, Boundary Layer, and Mesoscale Interactions with a Wind Farm. *Bull. Amer. Meteo. Soc.* 94: 655–672.

Rajewski DA, Takle ES, Lundquist JK, Prueger JH, Pfeiffer RL, Hatfield JL, Spoth KK, and Doorenbos RK 2014 Changes in fluxes of heat, H_2O, and CO_2 caused by a large wind farm. *Agric. For. Meteo.*, 194:175-187.

Skamarock WC, Klemp JB, Dudhia J, David OG, and Zhiquan L et al. 2021 A description of the Advanced Research WRF Version 4. *NCAR Technical Note*, NCAR/TN–556+STR.

St. Martin CM, Lundquist JK, and Handschy MA 2015 Variability of interconnected wind plants: correlation length and its dependence on variability time scale. *Environ. Res. Lett.*, 10(4):044004.

Stull RB 1988 An Introduction to boundary layer meteorology, Kluwer academic publishers, Netherlands.

Vanderwende BJ, Kosovi B, Lundquist JK, and Mirocha DJ 2016 Simulating effects of a wind-turbine array using LES and RANS. *J. Adv. Model. Ear. Syst*. 8(3):1376-1390.

Vanderwende BJ, and Lundquist JK 2012 The modification of wind turbine performance by statistically distinct atmospheric regimes. *Environ. Res. Lett.*, 7(3): 034035.

Volker PJ, Badger J, Hahmann AN, and Ott. S 2015 The explicit wake parametrisation V1.0: a wind farm parametrisation in the mesoscale model WRF. *Geosci. Model Dev*. 8(11):3715-3731.